CHEMISTRY
AN ASIAN JOURNAL
ACES
FULL PAPER

DOI: 10.1002/asia.201301289

Fluorine-Doped Fe_2O_3 as High Energy Density Electroactive Material for Hybrid Supercapacitor Applications

Kaliyappan Karthikeyan,[a, b] Samuthirapandian Amaresh,[a] Sol Nip Lee,[a] Vanchiappan Aravindan,[c] and Yun Sung Lee*[a]

Abstract: Nanostructured α-Fe_2O_3 with and without fluorine substitution were successfully obtained by a green route, that is, microwave irradiation. The hematite phase materials were evaluated as a high-performance electrode material in a hybrid supercapacitor configuration along with activated carbon (AC). The presence of fluorine was confirmed through X-ray photoelectron spectroscopy and transmission electron microscopy. Fluorine-doped Fe_2O_3 (F-Fe_2O_3) exhibits an enhanced pseudocapacitive performance compared to that of the bare hematite phase. The F-Fe_2O_3/AC cell delivered a specific capacitance of 71 $F g^{-1}$ at a current density of 2.25 $A g^{-1}$ and retained approximately 90% of its initial capacitance after 15000 cycles. Furthermore, the F-Fe_2O_3/AC cell showed a very high energy density of about 28 $W h kg^{-1}$ compared to bare hematite phase (~9 $W h kg^{-1}$). These data clearly reveal that the electrochemical performance of Fe_2O_3 can be improved by fluorine doping, thereby dramatically improving the energy density of the system.

Keywords: activated carbon · energy storage · fluorine doping · hybrid supercapacitor · iron oxide

Introduction

Due to the increasing awareness of global warming and depletion of oil resources, many efforts are being devoted to find alternative energy sources, especially for hybrid electric vehicles (HEVs) and large-scale consumer electronics applications.[1–4] Lithium-ion batteries (LIBs) are currently the best choice for such applications, but still several issues remain unsolved such as poor power density, safety issues, costs, performance, and the availability of lithium raw materials.[1] Electrochemical double-layer capacitors (EDLCs) represent one of the greatest innovations in the field of electrochemical energy storage.[1,5,6] Although EDLCs deliver a high power density, their energy density is highly limited because of the non-Faradaic reaction mechanism and water splitting issues when employed in an aqueous medium.[1,6] On the other hand, organic solutes provide a higher energy density; however, their poor conductivity and mobility obstruct the achievement of desirable values to drive such vehicles. Another approach to increase the energy density is the use of hybrid supercapacitors (HSCs), which consist of a double-layer carbon material in one electrode and pseudocapacitive or Faradaic materials in the other electrode. An example is the use of a pseudocapacitive electrode coupled with activated carbon (AC); however, in such a system the operating potential cannot be widened beyond 2 V in an aqueous medium.[7,8] As a result, the obtained energy density is not at the expected level. Therefore, we made an attempt to use organic solutes for increasing the energy density of an HSC. For such an assembly, AC is the unanimous choice because of its inherent properties like high surface area, high chemical and thermal stability, excellent conductivity, and low cost.[9,10] Therefore, the search for pseudocapacitance materials to replace the hydrous ruthenium oxide ($RuO_2 \cdot x H_2O$) electrode is highly warranted. Although such an electrode offers a very high specific capacitance (~720 $F g^{-1}$) with an excellent stability for prolonged cycling, the high cost of RuO_2 limits its use in large-scale applications.[5,11] Hence, inexpensive metal oxide alternatives to RuO_2 have become a major research area. Transition metal oxides such as MnO_2, NiO, Co_2O_3, V_2O_5, and SnO_2 have been identified as potential alternatives to RuO_2.[9,12–14] In spite of their excellent capacitive behavior, the inherent electronic conductivity and limited cycle life forbids their practical use. Iron oxides have been proposed as one of the attractive alternatives for HSCs because of their low cost, abundance, and eco-friendliness.[13,15] Iron oxides such as Fe_3O_4 and γ-Fe_2O_3 exhibit an excellent pseudocapacitive behavior with a specific capacitance in the range of 5–500 $F g^{-1}$

[a] Dr. K. Karthikeyan, S. Amaresh, S. N. Lee, Prof. Y. S. Lee
Faculty of Applied Chemical Engineering
Chonnam National University
Gwang-ju 500-757 (Korea)
E-mail: leeys@chonnam.ac.kr

[b] Dr. K. Karthikeyan
Department of Mechanical and Materials Engineering
The University of Western Ontario
London, Ontario, N6A 5B9 (Canada)

[c] Dr. V. Aravindan
Energy Research Institute @ NTU (ERI@N)
Nanyang Technological University
Research Techno Plaza, 50 Nanyang Drive, Singapore 637553 (Singapore)

Supporting information for this article is available on the WWW under http://dx.doi.org/10.1002/asia.201301289.

in alkaline medium, depending on the surface morphology, structure, and cell design. Recent studies clearly showed that the good capacitance behavior of α-Fe_2O_3 is strongly influenced by its surface arrangements/morphology, which completely depends on the preparation and processing parameters.[14] Although the superior capacitive properties of nanotubes and nanostructured α-Fe_2O_3 resulted from a large active surface area, which allows for more Faradaic reactions (on the surface) and a shorter pathway for rapid ion diffusion, the synthesis of those unique structures is quite complex and difficult to control during scale-up.[14] Moreover, high rate capabilities of those materials are not in an acceptable range, as the Fe-based materials exhibited a poor electronic conductivity and metastability, thus leading to large capacitance fading during prolonged cycling. Several attempts have been made to improve the electrochemical performance of α-Fe_2O_3 through the preparation of carbon composites, cationic doping, and the incorporation of a conducting polymer matrix into the hematite structure.[16–18] On the other hand, computational studies indicate that the partial replacement of oxygen by anions such as N^{3-}, S^{2-}, Cl^-, and F^- can effectively improve the rate capability.[19–23] In addition, anion doping for oxygen influenced the reduction of impedance and lattice changes during cycling, and significantly improved the cycle life as well.[24] Fluorine, which has a radius similar to that of oxygen, could be an adequate anion dopant due to its lower lattice distortion compared to the rest of the alternatives. Recently, many studies have been conducted on fluorine doping into metal oxides in order to enhance the electrochemical performance of LIBs and solar cells.[20,23,25] Furthermore, the presence of F-doping certainly suppresses the decomposition of the electrolyte and the subsequent formation of a thick solid electrolyte interphase (SEI), which certainly improves the stability of the electrolyte solution during prolonged cycling.[26] Nevertheless, the enhancement of pseudocapacitive properties of metal oxides in HSC applications by F^- substitution has so far not been reported. Herein, we have synthesized F-doped α-Fe_2O_3 using a simple microwave irradiation technique for the first time and examined its electrochemical performance in a HSC configured with an AC counter electrode in a non-aqueous medium in detail.

Results and Discussion

Figure 1a shows the XRD patterns of F-Fe_2O_3 and Fe_2O_3 powders. They agree with the formation of phase pure hematite (α-Fe_2O_3) structures without any impurity traces. The observed reflections are indexed according to the rhombohedral structure and consistent with the JCPDS data (card no. 33-0664). The observed sharp, intense reflections confirm the highly crystalline nature of the powders synthesized by microwave irradiation and subsequent heat treatment. The lattice parameter values calculated from the refinement data were found to be $a = 5.047$ Å and $c = 13.854$ Å for Fe_2O_3 and $a = 5.038$ Å and $c = 13.774$ Å for F-Fe_2O_3 phases. The small variation clearly indicates the influence of F-doping on the hematite phase and corroborates the stronger M–F bond as compared to the M–O bond. In addition, the small decrease in the lattice parameter values after F-doping is mainly attributed to the smaller radius of F^- (1.33 Å) ions compared to O^{2-} (1.40 Å). On the other hand, no noticeable changes in the XRD patterns were observed, which may reflect a low fluorine content. The crystallite sizes of hematite powders were calculated using Scherrer's equation and found to be about 20 and 40 nm for Fe_2O_3 and F-Fe_2O_3 phases, respectively. In order to confirm the presence of F^-in the hematite phase, the powders were analyzed by X-ray photoelectron spectroscopy (XPS). The core-level spectra of Fe 2p, O 1s, and F 1s for F-Fe_2O_3 and Fe_2O_3 phases are presented in Figure 1b–d. The core-level spectra of Fe 2p exhibit two characteristics peaks with corresponding binding energies of Fe $2p_{3/2}$ and Fe $2p_{1/2}$ at 711.1 and 724.2 eV, respectively, which correlate well with previously reported values of Fe^{3+} in α-Fe_2O_3.[27] As shown in Figure 1c, the core-level spectra of O 1s showed a dominant oxide peak at about 529.9 eV, which is the typical state of O^{2-} species in the α-Fe_2O_3 phase. The deconvoluted O 1s

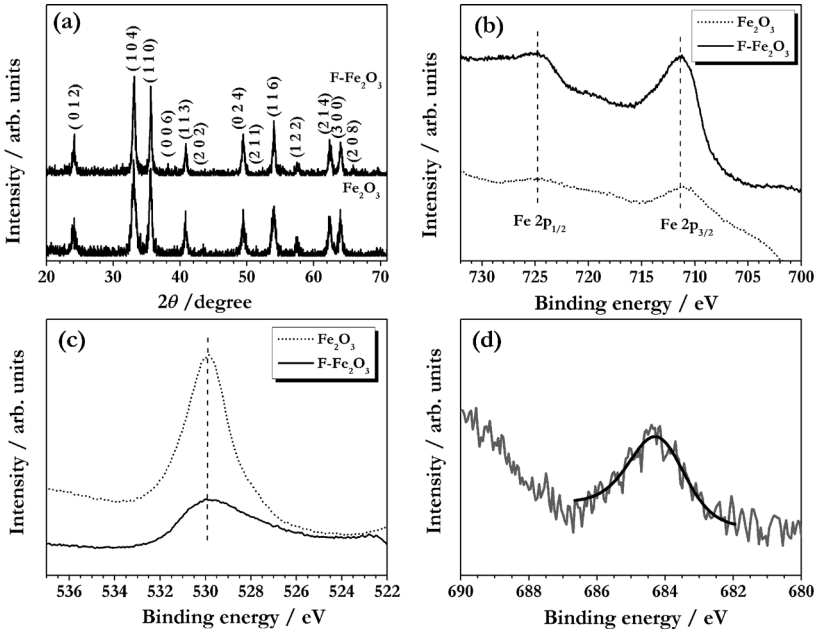

Figure 1. (a) XRD patterns of Fe_2O_3 and F-Fe_2O_3 materials prepared by using the microwave irradiation method. High-resolution XPS spectra of (b) Fe 2p and (c) O 1s of both Fe_2O_3 and F-Fe_2O_3 materials. (d) XPS spectrum of F 1s of F-Fe_2O_3 with fitting.

spectra showed the presence of Fe(OH), FeO(OH), C=O, OH, and H_2O, in the order of decreasing atomic percentages (Figure S1, Supporting Information).[28] Figure 1d shows the core-level XPS spectrum of F 1s of the F-Fe_2O_3 powder. Since the level of fluorine doping is low, it was expected that the peak would not be detectable due to noise; however a peak was observed and fitting of the F 1s spectrum clearly showed a binding energy at about 683 eV, which is close agreement with that of other metal fluorides. Generally, NiF_2 and MnF_2 exhibit binding energies (F 1s) between 648.5 and 685.9 eV, and thus the F 1s spectrum of F-Fe_2O_3 verified that fluorine has been successfully incorporated into the hematite lattice.[23,25] The FT-IR spectra also support the presence of F by exhibiting weak bands at 1023 cm^{-1} for F-Fe_2O_3 compared to bare hematite phase (Figure S2, Supporting Information).

The morphological features of bare and F-Fe_2O_3 powders were analyzed by transmission electron microscopy (TEM). Bare Fe_2O_3 exhibits an irregular particulate morphology and uneven distributions ranging from 20 to 30 nm (Figure 2a), whereas an increased particle size (40–50 nm) and well-defined surface morphologies were observed for F-Fe_2O_3 powders (Figure 2b). Similar changes in surface morphology

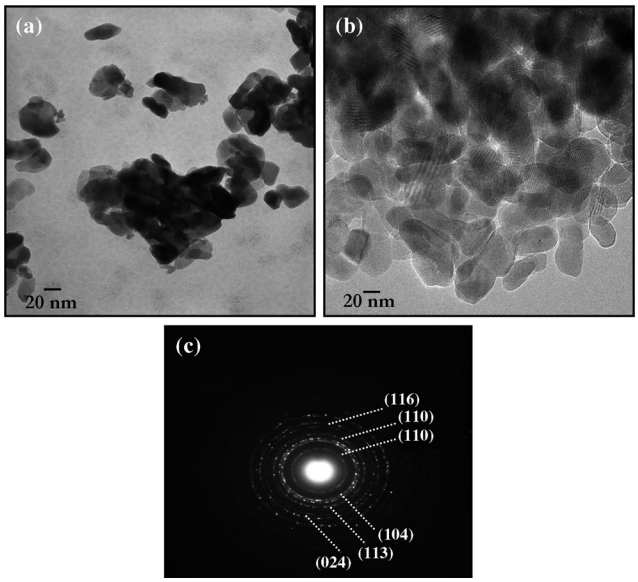

Figure 2. TEM images of (a) Fe_2O_3 and (b) F-Fe_2O_3 materials. (c) SAED pattern of F-Fe_2O_3 nanoparticles. Recorded diffraction rings are indexed with corresponding Miller indices.

were observed for F-doped spinel phase cathodes.[20,23,29] The changes in morphology after F doping slightly increase the agglomerated particles compared to bare Fe_2O_3, indicating an increase in tap density which certainly provides the high power capability of the system. The selected-area electron diffraction (SAED) pattern of F-Fe_2O_3 exhibits typical hexagonal characteristics, thus confirming that the fluorine-doped hematite nanoparticles are well crystallized (Figure 2c). In addition, elemental mapping and energy-dispersive X-ray (EDX) spectroscopy also confirms the presence of F in the hematite phase (Figure S3, Supporting Information). This clearly reveals that microwave irradiation is a suitable technique to enable homogeneous F-doping in hematite phase. It is worth mentioning that charge imbalances created from the replacement of O^{2-} ions by F^- ions are neutralized through the formation of surface-adsorbed hydroxy groups.

It is well known that the energy storage behavior of HSCs mainly depends on the mass balance between the individual electrodes since the applied current in an HSC will split based on the separate capacitive performance of the electrodes. Consequently, the mass balance between the electrodes is adjusted during the fabrication[30] of HSCs based on the electrochemical performance of such electrodes in a single electrode configuration (Li/Fe_2O_3 and Li/AC, where metallic lithium acts as counter and reference electrode). Figure S4 in the Supporting Information shows typical charge–discharge studies of Li/Fe_2O_3 and Li/AC cells at 7C rate (500 mA g^{-1}, calculated based on the discharge time of the half-cells). Based on the performance (a discharge capacity of ~189 and ~69 mA h g^{-1} was noted for F-Fe_2O_3 and AC, respectively), the mass loading of AC and F-Fe_2O_3 has been adjusted to 2.7:1. The electrochemical performances of bare and F-Fe_2O_3 were examined in HSC configurations along with AC anodes using cyclic voltammetric (CV) analysis between 0–3 V at different scan rates. Figure 3a clearly depicts the typical CV signatures of F-Fe_2O_3/AC and Fe_2O_3/AC cells recorded at a scan rate of 100 mV s^{-1}. The two HSC cells exhibited almost rectangular profiles with mirror-image characteristics, which is typical of ideal supercapacitors. In addition, the shape of CV curves for F-Fe_2O_3/AC and Fe_2O_3/AC cells revealed the capacitive characteristic of HSC cells distinct from an electric double-layer capacitor, which could be attributed to the combination of different energy storage mechanisms: a double-layer capacitance from the AC electrodes and a pseudocapacitive behavior from the Fe_2O_3 electrodes.[7,31] The CV traces also show that the current response of the cells remained constant during the anodic and cathodic scans; furthermore, the curves are almost symmetrical, indicating an excellent reversibility of the cells at the high scan rate of 100 mV s^{-1}. This satisfactory kinetic reactivity even at such a high scan rate makes these binary oxides promising as electrode materials for high-performance HSC applications.[8] Moreover, the enclosed area under the CV curves differs in that the F-Fe_2O_3/AC cell has a stronger current response than the Fe_2O_3/AC cell, thus indicating its superior energy storage property compared to bare hematite phase. The higher current response of F-Fe_2O_3/AC cell might be attributed to well-developed particles with largely exposed contact areas as well as a good contact towards the current collector.[32] The specific capacitance values for HSC cells were also calculated from the CV curves, and their relationship with the scan rates (Figure S5, Supporting Information) is presented in Figure 3b. As expected, a monotonous decline in the specific capacitance of the cells with increasing potential scan rates is clearly ob-

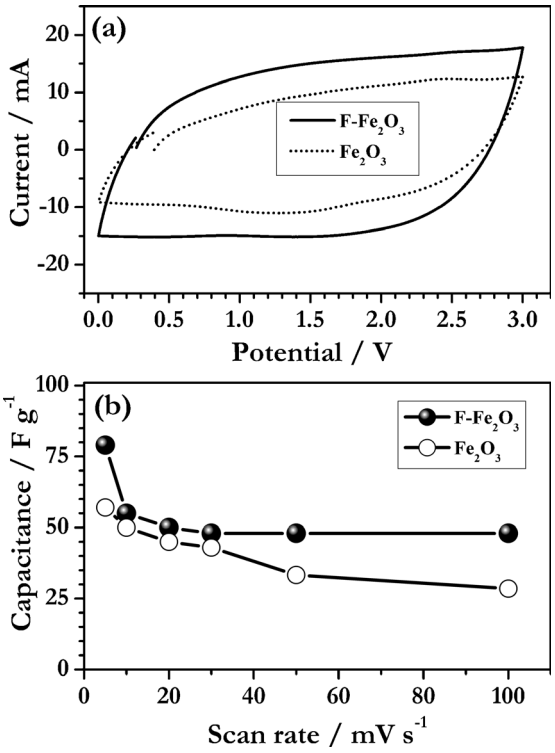

Figure 3. (a) CV traces of Fe_2O_3/AC and F-Fe_2O_3/AC HSC cells measured at a scan rate of 100 mV s^{-1} in the range of 0–3 V in a conventional organic electrolyte. (b) Plot of the specific capacitance as a function of scan rate.

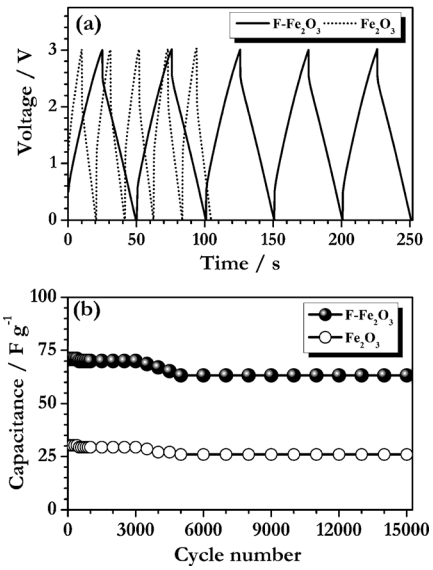

Figure 4. (a) Galvanostatic charge–discharge curves of Fe_2O_3/AC and F-Fe_2O_3/AC HSC cells recorded in the range of 0–3 V at a current density of 2.25 A g^{-1}. (b) Cycle life of the HSC cells.

served because of the kinetic and diffusion limitations. The Fe_2O_3/AC and F-Fe_2O_3/AC HSC cells delivered a maximum specific capacitance of 57 and 79 F g^{-1}, respectively, at a slow scan rate of 5 mV s^{-1}. Furthermore, when the scan rate was increased to 100 mV s^{-1}, the capacitance of Fe_2O_3/AC decreased to 29 F g^{-1}, whereas the F-Fe_2O_3/AC cell still delivered a capacitance of 48 F g^{-1} at the same scan rate. Possible reasons for the poor performance of the cell containing the bare Fe_2O_3 electrode may be a lower electronic transport as well as comparatively sluggish reaction kinetics on the surface at high scan rates.[16] On the other hand, the substitution of fluorine effectively suppressed the polarization of the electrodes and, therefore, an enhanced electrochemical performance is achieved with F-doping.[20]

The galvanostatic charge–discharge behavior of the HSC cells was recorded at various current densities, and the dependence of the capacitance as a function of current density is presented in Figure 4and in Figure S6, Supporting Information. As shown in these figures, the F-Fe_2O_3/AC HSC cell delivered an improved electrochemical performance compared to the HSC cell containing the bare hematite electrode. A high-rate performance with a prolonged cycle life is essential for any energy storage device for use in high-energy and high-power applications like HEVs.[2,4,8] Figure 4a shows the typical charge–discharge curves of HSC cells between 0 and 3 V at a current density of 2.25 A g^{-1} in 1:1 ethylene carbonate (EC)/dimethyl carbonate (DMC) electrolyte containing 1 M $LiPF_6$. From Figure 4a it is evident that charge and discharge curves of both cells are nearly symmetrically trilateral in shape, which indicates an excellent electrochemical reversibility of the cells irrespective of the applied current density. The slight distortion in the curves of the HSC is attributed to the combined characteristics of both redox and double-layer capacitors.[7] In addition, the HSC is experiencing a slight drop in potential (IR drop) that arises from the internal resistance of the electrodes and is known as ohmic drop. This ohmic drop involves the separation of an electrochemical double layer across the electrode/electrolyte interface and the redox component associated with the Faradic reaction of Fe_2O_3 electrodes.[32] Moreover, the F-Fe_2O_3/AC HSC cell showed a longer discharge time compared to Fe_2O_3/AC, thus suggesting that F^- doping effectively improved the electrochemical performance of the native hematite phase. The enhanced electrochemical behavior of the F-Fe_2O_3/AC HSC cell also resulted from the lower IR drop (Figure S7, Supporting Information), and the magnitude of the ohmic drop increased with increasing current density; for instance, an ohmic drop of 0.88 and 2 V is noted for F-Fe_2O_3/AC and Fe_2O_3/AC cells, respectively, at a current density of 2.25 A g^{-1}. The specific capacitance was calculated from the galvanostatic studies and its dependence on the cycle number is shown in Figure 4b. The F-Fe_2O_3/AC HSC delivered a specific capacitance of about 71 F g^{-1} at a current density of 2.25 A g^{-1} and retained approximately 90% of initial value (i.e., ~63 F g^{-1}) after 15000 cycles. On the other hand, the Fe_2O_3/AC HSC delivered about 30 F g^{-1} and maintained about 85% of the initial capacitance under the same testing conditions. The influence of fluorine doping on the electrochemical performance of the Fe_2O_3 electrode is illustrated by the following facts: 1) an increase in the electronic conductivity of the hematite phase (Fig-

ure 5b), 2) a more stable structure under high current testing owing to the strong M–F bond, and 3) an improved diffusion of Li^+ by fluorine doping (only on the surface, not to the bulk). Since the ionicity of F^- is high, it contributes to enhance the ionic motion in the F-Fe_2O_3 material.[20,21] The presence of fluorine on the electrode surface provides additional protection from attack by HF and thus decreased the electrolyte decomposition and subsequent formation of a thick SEI layer, which enhanced the cycling behavior at high current rates.[20,21]

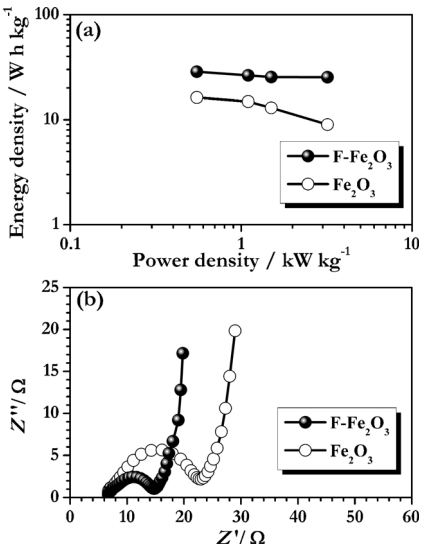

Figure 5. (a) Ragone plot of Fe_2O_3/AC and F-Fe_2O_3/AC HSC cells at different current densities. (b) Nyquist plots of Fe_2O_3/AC and F-Fe_2O_3/AC HSC cells recorded at an open circuit voltage between 100 kHz and 100 mHz.

Figure 5a presents the Ragone plot of the HSC cells with bare and F-Fe_2O_3 electrodes. Obviously, the F-Fe_2O_3/AC HSC exhibited a remarkable rate performance compared to the Fe_2O_3/AC cell. The F-Fe_2O_3/AC HSC delivered an energy density of about 28 W h kg^{-1} with a corresponding power density of 0.55 kW kg^{-1}, whereas an energy density of 16 W h kg^{-1} was only obtained for bare Fe_2O_3. Furthermore, the electrochemical parameters obtained for the F-Fe_2O_3/AC HSC cell is much higher than that of the Fe_2O_3/MWCNT (MWCNT = multi-walled carbon nanotube) cell reported by Zhao et al.[16] and that of other configurations such as $LiCrTiO_4$/AC (energy density of ~23 W h kg^{-1}),[33] V_2O_5/AC (18 W h kg^{-1}),[31] $LiTi_2(PO_4)_3$/AC (14 W h kg^{-1}),[34] $LiCoPO_4$/carbon nanofoam (13 W h kg^{-1}),[35] TiP_2O_7/AC (13 W h kg^{-1}),[36] and TiO_2-B/CNTs (12.5 W h kg^{-1}).[37] Figure 5b shows the Nyquist plots of the F-Fe_2O_3/AC and Fe_2O_3/AC HSC cells recorded at open circuit voltages between 100 mHz and 100 kHz. As expected, the Nyquist plots exhibited two main regions: a semicircle in the high-frequency region and an inclined line in the low-frequency region. The former is derived from the charge-transfer process across the electrode/electrolyte interface and is also known as the charge-transfer resistance (R_{ct}). The latter is associated with the diffusion-controlled process and called Warburg resistance.[38] The F-Fe_2O_3/AC cell displayed a much smaller R_{ct} value than the bare hematite phase electrode (9.5 vs. 19.3 Ω). The lower R_{ct} value is attributed to the fluorine doping into the Fe_2O_3 lattice, which contributed to the formation of uniform-sized particles, thereby improving the reaction kinetics and enhancing the electrochemical performance of F-Fe_2O_3/AC HSC. This clearly demonstrates that the substitution of fluorine plays an important role in increasing the electrical conductivity of the electrode material, which alleviates cell polarization during the cycling process. These results agree well with the data obtained in the CV and charge–discharge studies and also suggest the possibility of adopting fluorine-doped Fe_2O_3 as high-performance electrode in HSC applications.

Conclusions

The influence of fluorine doping in Fe_2O_3 materials for hybrid supercapacitor applications was investigated in combination with an activated carbon (AC) anode in a non-aqueous medium. The F-Fe_2O_3/AC HSC cell delivered a maximum specific capacitance of about 71 F g^{-1} and an energy density of about 28 W h kg^{-1}at a current density of 2.25 A g^{-1}. Furthermore, it was observed that the F-Fe_2O_3/AC HSC cell retained 90% of its initial value after 15000 cycles at the aforementioned current rate. The enhanced rate performance could be attributed to the lower impedance arising from fluorine doping, a lower ohmic drop, and an increase in the active sites for electrochemical reaction. This study thus suggests that F-doping by a green approach (i.e., microwave irradiation) is an appropriate way to tune a transition metal oxide into an electroactive material with high energy density. This green approach could likely be extended to other oxides.

Experimental Section

F-doped hematite (F-Fe_2O_3) nanoparticles were synthesized in aqueous solution using microwave irradiation. In a typical procedure, appropriate amounts of iron nitrate (Junsei, Japan), ammonium fluoride (Alfa Aesar, USA), and urea (Junsei, Japan) were dissolved in distilled water (10 mL) and continuously stirred for 30 min at room temperature. The solution was heated heated in a microwave oven (700 W, Daewoo, Korea) for 15 min and cooled down to room temperature. The resulting brownish-black solid product was washed with deionized water and dried at 60 °C for 12 h. Finally, F-Fe_2O_3 was obtained by heating the powders in a box furnace at 350 °C for 2 h. For comparison, bare Fe_2O_3 was also prepared using the same method without adding ammonium fluoride. The amount of fluorine in the F-Fe_2O_3 sample was measured using XPS analysis to be about 1.5 atomic percent.

The crystallographic structures of the samples were analyzed by X-ray diffraction (XRD) using $Cu_{K\alpha}$ radiation (Rint 1000, Rigaku, Japan). X-ray photoelectron spectroscopy (XPS) was conducted with monochromatic $Al_{K\alpha}$ radiation ($h\nu$ = 1486.6 eV, MultiLab 2000, Thermo Scientific, UK). Morphological features of the samples were observed by transmission electron microscopy (TEM, TecnaiF20, Philips, Netherlands). Fouri-

er transform infra-red (FT-IR) spectroscopy was conducted using an IR-Prestige-21 spectrometer (Shimadzu, Japan).

The electrochemical performance of HSC cells was measured using CR2032 coin cells in the range of 0–3 V using a battery tester (WBCS 3000, Won-A-Tech, Korea). Composite cathodes were formulated with 75% of active materials (F-Fe_2O_3 or Fe_2O_3), 15% of Ketzen black (KB), and 10% of teflonized acetylene black (TAB) using ethanol. The slurry was then pressed on a 200 mm^2 nickel steel mesh current collector and dried at 160 °C for 4 h in a vacuum oven. The same procedure was repeated to fabricate AC electrodes. The test cells were constructed in an argon-filled glove box by compressing the F-Fe_2O_3 or Fe_2O_3 electrode and AC counter electrode separated by a porous polypropylene film (Celgard 3401, USA) and filled with 1 M $LiPF_6$ in 1:1 ethylene carbonate (EC)/dimethyl carbonate (DMC) as electrolyte solution. Cyclic voltammetry (CV) and electrochemical impedance spectroscopy (EIS) studies were performed using a SP-150 electrochemical analyzer (Bio-Logic, France). The specific capacitance, internal resistance, energy density, and power density of the HSC were calculated using the following standard formulas:[31–34,36]

$$\text{Specific capacitance } (\mathrm{F\,g^{-1}}) = 4\,(I \times t/V \times m) \quad (1)$$

$$\text{Internal resistance } (\Omega) = (V_{\text{charge}} - V_{\text{discharge}})/I \quad (2)$$

$$\text{Power density } (\mathrm{W\,kg^{-1}}) = I \times V/m \quad (3)$$

$$\text{Energy density } (\mathrm{W\,h\,kg^{-1}}) = \text{power density} \times t/3600 \quad (4)$$

where V_{charge} and $V_{\text{discharge}}$ are the potentials at the end of charging and at the beginning of discharging after the potential drop, respectively, I is the applied current, V is the average cell potential ($0+3/2=1.5$ V), t is the discharge time, and m is the total mass of the active materials.

Acknowledgements

This research was supported by Basic Science Research Program through the National Research Foundation of Korea (NRF) funded by the Ministry of Education (NRF-2009-0094055).

[1] N.-S. Choi, Z. Chen, S. A. Freunberger, X. Ji, Y.-K. Sun, K. Amine, G. Yushin, L. F. Nazar, J. Cho, P. G. Bruce, *Angew. Chem.* **2012**, *124*, 10134–10166; *Angew. Chem. Int. Ed.* **2012**, *51*, 9994–10024.
[2] V. Aravindan, J. Gnanaraj, Y.-S. Lee, S. Madhavi, *J. Mater. Chem. A* **2013**, *1*, 3518–3539.
[3] M. M. Thackeray, C. Wolverton, E. D. Isaacs, *Energy Environ. Sci.* **2012**, *5*, 7854–7863.
[4] E. J. Cairns, P. Albertus, *Annu. Rev. Chem. Biomol. Eng.* **2010**, *1*, 299–320.
[5] K. Naoi, P. Simon, *Electrochem. Soc. Interface* **2008**, *17*, 34–37.
[6] P. Simon, Y. Gogotsi, *Nat. Mater.* **2008**, *7*, 845–854.
[7] W. F. Mak, G. Wee, V. Aravindan, N. Gupta, S. G. Mhaisalkar, S. Madhavi, *J. Electrochem. Soc.* **2012**, *159*, A1481–A1488.
[8] "Asymmetric and Hybrid Devices in Aqueous Electrolytes": T. Brousse, D. Bélanger, D. Guay in *Supercapacitors: Materials, Systems, and Applications* (Eds.: F. Béguin, E. Frąckowiak), Wiley-VCH, Weinheim **2013**, pp. 257–288.
[9] E. Frackowiak, F. Béguin, *Carbon* **2001**, *39*, 937–950.
[10] "Electrical Double-Layer Capacitors and Carbons for EDLCs": P. Simon, P.-L. Taberna, F. Béguin in *Supercapacitors: Materials, Systems, and Applications* (Eds.: F. Béguin, E. Frąckowiak), Wiley-VCH, Weinheim, **2013**, pp. 131–165.
[11] "Li-Ion-Based Hybrid Supercapacitors in Organic Medium": K. Naoi, Y. Nagano in in *Supercapacitors: Materials, Systems, and Applications* (Eds.: F. Béguin, E. Frąckowiak), Wiley-VCH, Weinheim, **2013**, pp. 239–256.
[12] E. Frackowiak in *Electrode Materials with Pseudocapacitive Properties*, Wiley-VCH, Weinheim, **2013**, pp. 207–237.
[13] C. D. Lokhande, D. P. Dubal, O.-S. Joo, *Curr. Appl. Phys.* **2011**, *11*, 255–270.
[14] Q. Qu, S. Yang, X. Feng, *Adv. Mater.* **2011**, *23*, 5574–5580.
[15] M.-S. Wu, R.-H. Lee, *J. Electrochem. Soc.* **2009**, *156*, A737–A743.
[16] X. Zhao, C. Johnston, P. S. Grant, *J. Mater. Chem.* **2009**, *19*, 8755–8760.
[17] X. Xia, Q. Hao, W. Lei, W. Wang, D. Sun, X. Wang, *J. Mater. Chem.* **2012**, *22*, 16844–16850.
[18] M. Mallouki, F. Tran-Van, C. Sarrazin, P. Simon, B. Daffos, A. De, C. Chevrot, J. F. Fauvarque, *J. Solid State Electrochem.* **2007**, *11*, 398–406.
[19] N. T. Hahn, C. B. Mullins, *Chem. Mater.* **2010**, *22*, 6474–6482.
[20] G. G. Amatucci, N. Pereira, *J. Fluorine Chem.* **2007**, *128*, 243–262.
[21] T. Mueller, G. Hautier, A. Jain, G. Ceder, *Chem. Mater.* **2011**, *23*, 3854–3862.
[22] K.-S. Park, P. Xiao, S.-Y. Kim, A. Dylla, Y.-M. Choi, G. Henkelman, K. J. Stevenson, J. B. Goodenough, *Chem. Mater.* **2012**, *24*, 3212–3218.
[23] G. G. Amatucci, N. Pereira, T. Zheng, J.-M. Tarascon, *J. Electrochem. Soc.* **2001**, *148*, A171–A182.
[24] S. B. Lee, S. H. Cho, V. Aravindan, H. S. Kim, Y. S. Lee, *Bull. Korean Chem. Soc.* **2009**, *30*, 2223–2226.
[25] J. Hu, R. G. Gordon, *Solar Cells* **1991**, *30*, 437–450.
[26] Z.-S. Wu, L. Xue, W. Ren, F. Li, L. Wen, H.-M. Cheng, *Adv. Funct. Mater.* **2012**, *22*, 3290–3297.
[27] C. Pereira, A. M. Pereira, P. Quaresma, P. B. Tavares, E. Pereira, J. P. Araujo, C. Freire, *Dalton Trans.* **2010**, *39*, 2842–2854.
[28] S. W. Lee, N. Yabuuchi, B. M. Gallant, S. Chen, B. S. Kim, P. T. Hammond, Y. Shao-Horn, *Nat. Nanotechnol.* **2010**, *5*, 531–537.
[29] S.-W. Oh, S.-H. Park, J.-H. Kim, Y. C. Bae, Y.-K. Sun, *J. Power Sources* **2006**, *157*, 464–470.
[30] V. Khomenko, E. Raymundo-Pinero, F. Beguin, *J. Power Sources* **2006**, *153*, 183–190.
[31] V. Aravindan, Y. L. Cheah, W. F. Mak, G. Wee, B. V. R. Chowdari, S. Madhavi, *ChemPlusChem* **2012**, *77*, 570–575.
[32] K. Karthikeyan, V. Aravindan, S. Lee, I. Jang, H. Lim, G. Park, M. Yoshio, Y. Lee, *J. Power Sources* **2010**, *195*, 3761–3764.
[33] V. Aravindan, W. Chuiling, S. Madhavi, *J. Mater. Chem.* **2012**, *22*, 16026–16031.
[34] V. Aravindan, W. Chuiling, M. V. Reddy, G. V. S. Rao, B. V. R. Chowdari, S. Madhavi, *Phys. Chem. Chem. Phys.* **2012**, *14*, 5808–5814.
[35] R. Vasanthi, D. Kalpana, N. Renganathan, *J. Solid State Electrochem.* **2008**, *12*, 961–969.
[36] V. Aravindan, M. V. Reddy, S. Madhavi, S. G. Mhaisalkar, G. V. Subba Rao, B. V. R. Chowdari, *J. Power Sources* **2011**, *196*, 8850–8854.
[37] Q. Wang, Z. Wen, J. Li, *Adv. Funct. Mater.* **2006**, *16*, 2141–2146.
[38] V. Aravindan, K. Karthikeyan, K. S. Kang, W. S. Yoon, W. S. Kim, Y. S. Lee, *J. Mater. Chem.* **2011**, *21*, 2470–2475.

Received: September 23, 2013
Revised: November 17, 2013
Published online: December 17, 2013